

AB

SLAC-PUB-7444
 Princeton/HEP/97-4
 UR-1498 ER/40685/902
 UTHEP-97-0301

Positron Production in Multiphoton Light-by-Light Scattering*

presented by

Christian Bula

for the E-144 Collaboration:

C. Bamber^{2,†}, S.C. Berridge⁵, S.J. Boege^{2,‡}, W.M. Bugg⁵, C. Bula¹,
 D.L. Burke⁴, R.C. Field⁴, G. Horton-Smith⁴, T. Koffas², T. Kotseroglou^{2,4},
 K.T. McDonald¹, A.C. Melissinos², D.D. Meyerhofer^{2,3}, E.J. Prebys¹, W. Ragg^{2,§},
 D.A. Reis², K. Shmakov⁵, J.E. Spencer⁴, D. Walz⁴ and A.W. Weidemann⁵

¹Joseph Henry Laboratories, Princeton University, Princeton, NJ 08544

²Dept. of Physics and Astronomy, ³Dept. of Mechanical Engineering,
 University of Rochester, Rochester, NY 14627

⁴Stanford Linear Accelerator Center, Stanford University, Stanford, CA 94309

⁵Dept. of Physics and Astronomy, University of Tennessee, Knoxville, TN 37996

Abstract. A signal of 106 ± 14 positrons above background has been observed in collisions of a low-emittance 46.6-GeV electron beam with terawatt pulses from a Nd:glass laser at 527 nm wavelength in an experiment at the Final Focus Test Beam at SLAC. Peak laser intensities of $\sim 1.3 \times 10^{18}$ W/cm² have been achieved corresponding to a value of 0.3 for the parameter $\Upsilon = \mathcal{E}^*/\mathcal{E}_{\text{crit}}$ where $\mathcal{E}^* = 2\gamma\mathcal{E}_{\text{lab}}$ is the electric field strength of the laser transformed to the rest frame of the electron beam and $\mathcal{E}_{\text{crit}} = m^2c^3/e\hbar = 1.3 \times 10^{16}$ V/cm is the QED critical field strength. The positrons are interpreted as arising from a two-step process in which laser photons are backscattered to GeV energies by the electron beam followed by a collision between the high-energy photon and several laser photons to produce an electron-positron pair. These results are the first laboratory evidence for a light-by-light scattering process involving only real photons.

(Contributed to the Proceedings of the Symposium on New Modes of Particle Accelerations - Techniques and Sources, Santa Barbara, CA, August 19-23, 1996.)

* Work supported in part by the Department of Energy grants DE-FG02-91ER40671, DE-FG02-91ER40685, DE-FG05-91ER40627 and contract DE-AC03-76SF00515.

† Present address: Hughes Leitz Optical Technologies Ltd., Midland, Ontario, L4R 2H2, Canada.

‡ Present address: Lawrence Livermore National Laboratory, Livermore, CA 94551.

§ Present address: Panoramastrasse 8, 78589 Durbheim, Germany.



sw 9736

INTRODUCTION

Following the discovery of the positron by Anderson in 1932 [1], Bethe and Heitler [2] provided a theory of the production of electron-positron pairs as arising from the interaction of a real photon with a virtual photon of the electromagnetic field of a nucleus. Shortly thereafter, Breit and Wheeler [3] calculated the cross section for production of an electron-positron pair in the collision of two real photons,

$$\omega_1 + \omega_2 \rightarrow e^+ e^-, \quad (1)$$

to be of order r_e^2 , where r_e is the classical electron radius. While pair creation by real photons is believed to occur in astrophysical processes [4] it has not been observed in the laboratory up to the present.

After the invention of the laser in 1960 the prospect of intense laser beams led to reconsideration of the Breit-Wheeler process by Reiss [5] and others [6,7]. Of course, for production of an electron-positron pair the center-of-mass energy of the scattering photons must be at least $2mc^2 \approx 1$ MeV. This can be achieved by scattering a laser beam against a high-energy photon beam created, for example, by backscattering the laser beam off a high-energy electron beam [8]. With laser light of wavelength 527 nm (energy 2.35 eV), a photon of energy 109 GeV would be required for reaction (1) to proceed. However, with an electron beam of energy 46.6 GeV as available at the Stanford Linear Accelerator Center (SLAC) the maximum Compton-backscattered photon energy from a 527-nm laser is only 29.2 GeV.

In strong laser fields the interaction need not be limited to initial states with two photons [5], but rather the number of interacting photons becomes large as the dimensionless, invariant parameter

$$\eta = \frac{e\mathcal{E}_{\text{rms}}}{m\omega_0 c} = \frac{e\mathcal{E}_{\text{rms}}\lambda_0/2\pi}{mc^2} = \frac{e\sqrt{\langle A_\mu A^\mu \rangle}}{mc^2} \quad (2)$$

approaches and exceeds unity. In this, the laser beam has laboratory frequency ω_0 , wavelength λ_0 , root-mean-square electric field \mathcal{E}_{rms} , and four-vector potential A_μ ; e and m are the charge and mass of the electron, respectively, and c is the speed of light. Thus the multiphoton Breit-Wheeler reaction,

$$\omega + n\omega_0 \rightarrow e^+ e^-, \quad (3)$$

becomes accessible for $n \geq 4$ laser photons of wavelength 527 nm colliding with a photon with $\hbar\omega = 29$ GeV.

For photons of wavelength 527 nm a value of $\eta = 1$ corresponds to laboratory field strength of $\mathcal{E}_{\text{lab}} = 6 \times 10^{10}$ V/cm and intensity $I = 10^{19}$ W/cm². Such

intensities are now practical in tabletop laser systems based on chirped-pulse amplification [9].

When a laser field of strength \mathcal{E}_{lab} is viewed in the rest frame of a relativistic, counter-propagating particle with laboratory energy E and Lorentz factor $\gamma = E/mc^2 \gg 1$ the laser field strength appears boosted to $\mathcal{E}^* = 2\gamma\mathcal{E}_{\text{lab}}$. For example, a 46.6-GeV electron has $\gamma = 9 \times 10^4$ so if it collides head on with a 527-nm laser pulse of strength $\eta = 1$ the field in the electron's rest frame is $\mathcal{E}^* = 1.1 \times 10^{16}$ V/cm. This is close to the quantum electrodynamic (QED) critical field strength $\mathcal{E}_{\text{crit}} = m^2c^3/e\hbar = 1.3 \times 10^{16}$ V/cm at which the energy gain of an electron accelerating over a Compton wavelength is its rest energy, and at which a static electric field would spontaneously break down into electron-positron pairs [10-12].

Indeed, the predicted rates [5-7] for reaction (3) become large only when the dimensionless invariant

$$\Upsilon = \frac{\mathcal{E}^*}{\mathcal{E}_{\text{crit}}} = \frac{\sqrt{(F_{\mu\nu}p^\nu)^2}}{mc^2\mathcal{E}_{\text{crit}}} \quad (4)$$

approaches unity. Here $F_{\mu\nu}$ is the laboratory electromagnetic field tensor of the laser beam and p^ν is the energy-momentum 4-vector of the high-energy electron. For given electron and photon energies E and ω_0 the parameters η and Υ are not independent, and for $E = 46.6$ GeV and $\hbar\omega_0 = 2.35$ eV they are related by $\Upsilon = 0.84 \eta$.

In reaction (3) where several laser photons interact at once it is useful to consider the interaction as taking place with the field rather than individual quanta. This leads to an interpretation of the pair creation as a barrier-penetration process. A virtual electron-positron pair in the vacuum can materialize if the charges separate by distance d sufficient to extract energy $2mc^2$ from the field, *i.e.* if $e\mathcal{E}d = 2mc^2$. The probability of penetration of this 'barrier' of thickness d is proportional to $\exp(-2d/\lambda_C) = \exp(-4m^2c^3/e\hbar\mathcal{E}) = \exp(-4/\Upsilon)$, where λ_C is the Compton wavelength of the electron. A more complete calculation of this process [10-12] indicates that the rate for pair production ($R_{e^+e^-}$) is

$$R_{e^+e^-} \propto \exp(-\pi/\Upsilon). \quad (5)$$

In addition to pursuing the basic physics program outlined above, our experiment provides a demonstration of the technology for $e\text{-}\gamma$ and $\gamma\text{-}\gamma$ collider options [13], leading to measurements of the γWW coupling via the reaction $e\gamma \rightarrow W\nu$ [14,15], *etc.* Also, copious production of positrons in $e\text{-}\gamma$ collisions could provide a low-emittance positron source due to the absence of final-state Coulomb scattering [16].

EXPERIMENTAL SETUP

We have performed an experimental study of strong-field QED in the collision of a 46.6-GeV electron beam with terawatt pulses from a frequency doubled Nd:glass laser. A schematic diagram of the experiment is shown in Fig. 1. The apparatus was designed to detect electrons that undergo nonlinear Compton scattering,

$$e + n\omega_0 \rightarrow e' + \omega, \quad (6)$$

as well as positrons from the two-step process of reaction (6) followed by reaction (3). Measurements of reaction (6) have been reported elsewhere [17,18].

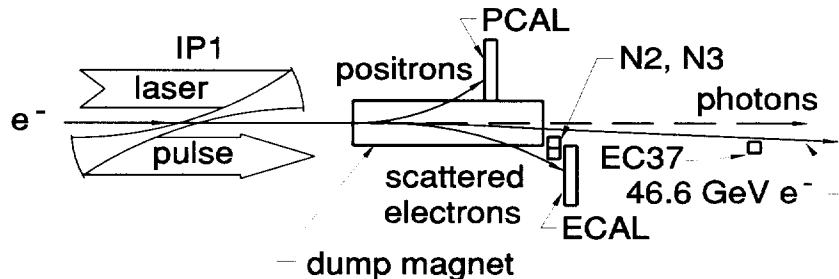


FIGURE 1: Schematic layout of the experiment.

The experiment was carried out in the Final Focus Test Beam (FFTB) at SLAC [19]. The laser beam was focused onto the electron beam by an off-axis parabolic mirror of 30-cm focal length with a 17° crossing angle at the interaction point, IP1, 10 m downstream of the Final Focus.

The laser was a 1.5-ps (fwhm), chirped-pulse-amplified Nd:glass terawatt system with a relatively high repetition rate of 0.5 Hz achieved by a final laser amplifier with slab geometry [18,20,21]. The laser-oscillator mode locker was synchronized to the 476-MHz drive of the SLAC linac klystrons with an observed jitter between the laser and linac pulses of 2 ps (rms) [22]. The spatial and temporal overlap of the electron and laser beams was optimized by observing the Compton scattering rate in the EC37, N2, N3 and ECAL detectors during horizontal, vertical, and time scans of one beam across the other [21].

The intensity of the laser at the focus was determined from measurements of the laser energy, focal-spot area, and pulse width. The uncertainty in the pulse width was $\pm 35\%$ in that measurements could be made only occasionally with a single-shot autocorrelator. Fluctuations on the energy probe calibration led to a $\pm 20\%$ uncertainty in the energy measurement. The focal spot area at IP1 was measured by reimaging the focus of the laser on a CCD. Because of laser light scattering, filtering, and a non-Gaussian shape of the focal spot

the uncertainty in the area was $\pm 30\%$. The overall uncertainty in the laser intensity as determined by these diagnostic devices was therefore $\pm 50\%$.

The peak focused laser intensity was obtained for green pulses of energy $U = 650$ mJ, focal area $A \equiv 2\pi\sigma_x\sigma_y = 30 \mu\text{m}^2$, and pulse width $\Delta t = 1.6$ ps (fwhm), for which $I = U/A\Delta t \approx 1.3 \times 10^{18}$ W/cm² at $\lambda_0 = 527$ nm, corresponding to values of $\eta = 0.36$ and $\Upsilon = 0.3$.

The electron beam was operated at 10-30 Hz with an energy of 46.6 GeV and emittances $\epsilon_x = 3 \times 10^{-10}$ m-rad and $\epsilon_y = 3 \times 10^{-11}$ m-rad. The beam was tuned to a focus with typically $\sigma_x = 25 \mu\text{m}$ and $\sigma_y = 40 \mu\text{m}$ at the laser-electron interaction point. The electron bunch length was expanded to 3 ps (rms) to minimize the effect of the time jitter between the laser and electron pulses. Typical bunches contained 7×10^9 electrons. However, since the electron beam was significantly larger than the laser focal area only a small fraction of the electrons crossed through the peak field region.

A string of permanent magnets after the collision point deflected the electron beam downwards by 20 mrad. Electrons and positrons of momenta less than 20 GeV were deflected by the magnets into two Si-W calorimeters (ECAL and PCAL) as shown in Fig. 1. The calorimeters were made of alternating layers of silicon (300 μm) and tungsten (one radiation length) and measured electromagnetic shower energies with resolution $\sigma_E/E \approx 19\%/\sqrt{E[\text{GeV}]}$ (plus a constant electronic noise of 250 MeV). Each layer of silicon was divided into horizontal rows and 4 vertical columns of 1.6×1.6 cm² active area cells, which allowed the determination of isolated shower positions with resolution of 2 mm.

The Si-W calorimeters were calibrated in parasitic running of the FFTB to the SLC program in which linac-halo electrons of energies between 5 and 25 GeV were transmitted by the FFTB when the latter was tuned to a lower energy. The number of such electrons varied between 1 and 100 per pulse, which provided an excellent calibration of the ECAL and PCAL over a wide dynamic range. The calibration runs also confirmed the magnetic-field maps of the FFTB dump magnets that are used in our spectrometer.

Electrons scattered via reaction (6) for $n = 1, 2$ and 3 laser photons were measured in gas Čerenkov counters labeled EC37, N2 and N3 in Fig. 1. These counters were used to monitor the quality of the e -laser beam overlap and to extract the field intensity at the laser focus on each shot. We used detectors based on Čerenkov radiation because of their insensitivity to major sources of low-energy background, such as beam scraping and (in the case of N2 and N3) recoil electrons produced by Compton scattered electrons hitting beamline components. EC37 was calibrated by inserting a thin foil in the electron beam at IP1. The momentum acceptance and efficiency of the counters N2 and N3 were measured with the parasitic electron beam by comparison with the previously calibrated ECAL.

RESULTS

We used the PCAL calorimeter to search for positrons produced at IP1. Because of the high rate of electrons in the ECAL calorimeter from Compton scattering it was not possible to identify the electron partners of the positrons.

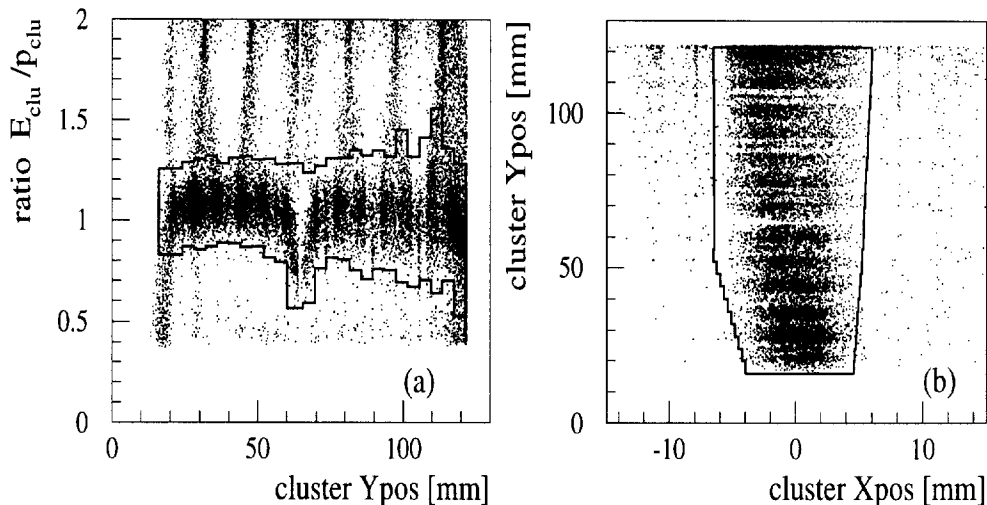


FIGURE 2: Cluster densities from Bethe-Heitler positrons produced by a wire at IP1. The solid line shows the signal region for positron candidates. (a) Ratio of cluster energy to momentum *vs.* vertical impact position. The low ratios at the center of PCAL are caused by a 1.5-mm-wide inactive gap. Similarly, at the top and bottom of PCAL a part of the shower energy is lost due to leakage out of PCAL. Two simultaneous showers separated by less than a cell caused the clusters with $E_{\text{clu}}/P_{\text{clu}} \sim 2$. (b) Cluster position in PCAL.

The response of PCAL to positrons originating at IP1 was studied by inserting a wire at IP1 to produce Bethe-Heitler e^+e^- pairs. These data were used to develop an algorithm to group contiguous PCAL cells containing energy deposits into ‘clusters’ representing positron candidates. The clusters were characterized by their position in the horizontal (X_{pos}) and vertical (Y_{pos}) direction and their total energy deposit E_{clu} . Using the field maps of the magnets downstream of IP1, the vertical impact position was translated into the corresponding momentum P_{clu} which could be compared to the cluster energy. Fig. 2 shows the density of clusters produced by the wire in the two planes $E_{\text{clu}}/P_{\text{clu}}$ *vs.* Y_{pos} and Y_{pos} *vs.* X_{pos} . Only clusters within the signal regions bounded by solid lines in Fig. 2 were counted as positron candidates.

We collected data at various laser intensities. The data from collisions with poor e -laser beam overlap were discarded. Also, events with anomalous values

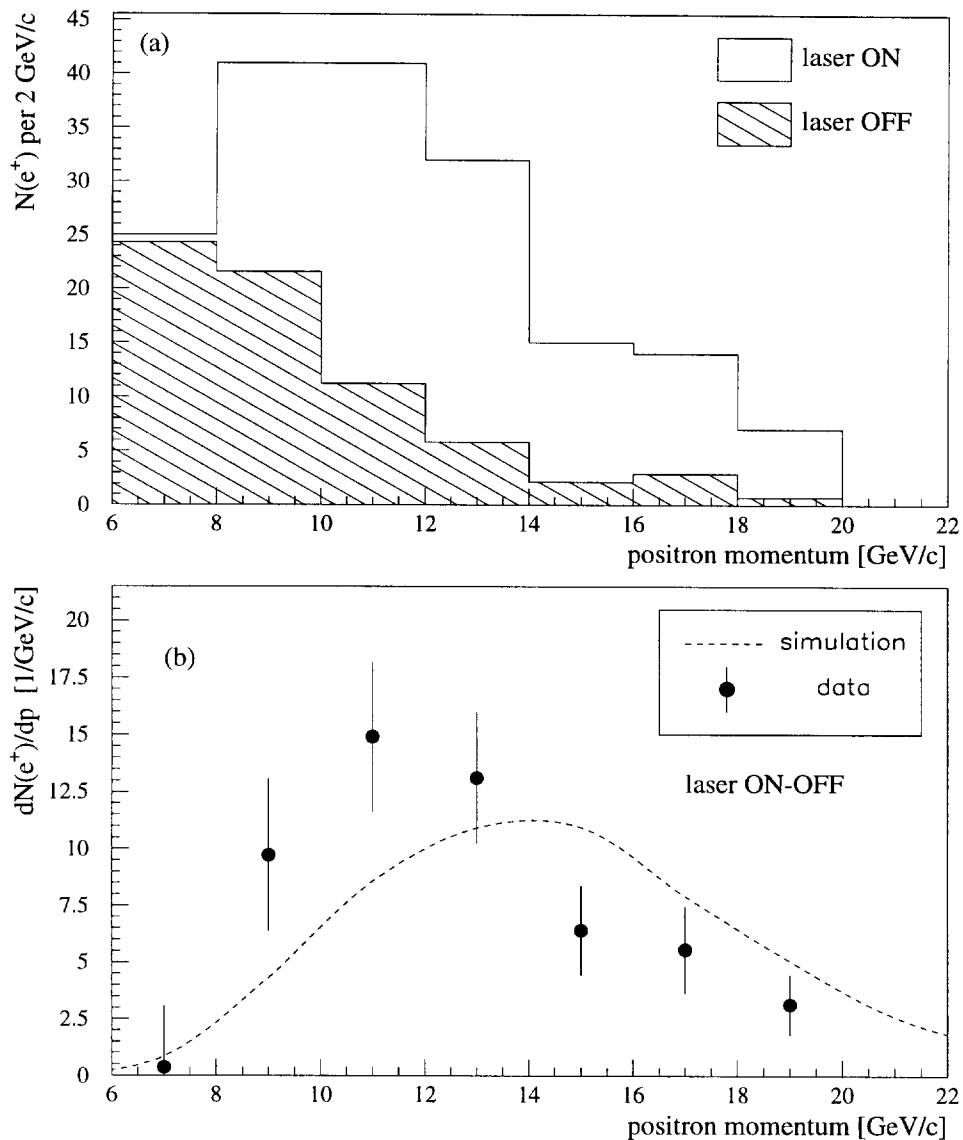


FIGURE 3: (a) Number of positron candidates *vs.* momentum for laser-on pulses and for laser-off pulses (hatched distribution, scaled to the number of laser-on pulses). (b) Spectrum of signal positrons obtained by subtracting the laser-off from the laser-on distribution. The dashed line shows the expected momentum spectrum from the model calculation. PCAL cluster positions have been converted to positron momentum via knowledge of the field in the magnetic spectrometer.

for any of the measured electron or laser beam parameters were removed from the data sample. The number of positron candidates observed in the remaining 21,962 laser shots is 175 ± 13 and is shown as the upper distribution in Fig. 3(a) as a function of cluster momentum.

Positrons were also produced in showers of lost electrons upstream of the e -laser interaction point. The rate of these background positrons was studied in 121,216 electron-beam pulses when the laser was off, yielding a total of 379 ± 19 positron candidates. Fig. 3(a) shows the momentum spectrum of these candidates as the hatched distribution, which has been scaled by 0.181, this being the ratio of the number of laser-on to laser-off pulses. After subtracting the laser-off distribution from the laser-on distribution we obtain the signal spectrum shown in Fig. 3(b) whose integral is 106 ± 14 positrons. The statistical significance of this result, by itself, is in excess of seven standard deviations. Even more significantly the momentum distribution of the observed positrons and the dependence of the rate on the laser intensity confirm that the positrons originate from light-by-light scattering, as discussed below.

We have modeled the pair production as the two-step process corresponding to reaction (6) followed by reaction (3). We followed the formalism of Ref. [6] for linearly polarized light as used in the experiment. By numerical integration over space and time in the e -laser interaction region we account for both the production of the high-energy photon (through a single or multiphoton interaction) and its subsequent multiphoton interaction within the same laser focus to produce the pair. Further Compton scatters of the positron (or electron) are also taken into account. The positron spectrum predicted by this calculation is shown as the dashed line in Fig. 3(b) and is in reasonable agreement with the data.

As mentioned before, several laser photons are needed to produce an e^+e^- pair under the present experimental conditions. The numerical simulation of the two-step Breit-Wheeler process, (6) followed by (3), indicates that the average number n of photons absorbed from the laser field in the second step is between 4 and 5 for a peak field intensity $\Upsilon \leq 0.35$. Fig. 4 shows the probability distribution of n for $\Upsilon = 0.3$ at the laser focus.

For an additional determination of the laser intensity we made use of N_1 , N_2 and N_3 , the numbers of electrons intercepted by the gas Čerenkov counters EC37, N2 and N3, of first-, second- and third-order Compton scattering, respectively. In principle, the field intensity could be extracted from each of these monitors. However, the result is more stable against various experimental uncertainties such as e -laser timing jitter if it is extracted only from ratios of the monitor rates. For $\eta^2 \ll 1$, the field intensity is approximately given by

$$\eta^2 = k_1 \cdot \frac{N_2}{N_1}, \quad \text{and} \quad \eta^2 = k_2 \cdot \frac{N_3}{N_2}. \quad (7)$$

The parameters k_1 and k_2 depend on the acceptance and efficiency of the

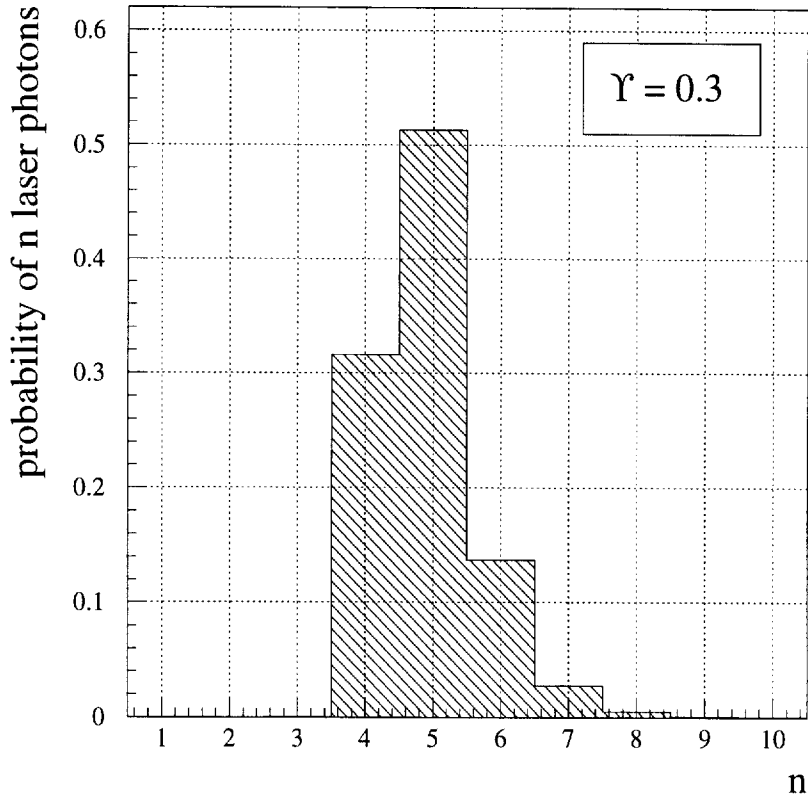


FIGURE 4: Calculated probability distribution of the number n of photons absorbed from the laser field in the second step of the two-step Breit-Wheeler pair creation process. A field intensity of $\Upsilon = 0.3$ at the laser focus was used for the simulation.

counters as well as the spectrum of scattered electrons and were calculated over the relevant range of η^2 values by the numerical simulation. We fit the observed N_i to ideal values subject to the constraint $N_2^2 = (k_2/k_1)N_1N_3$ obtained from Eq. (7). Then the fitted N_i were used to determine η and Υ for each laser shot with an average precision of 13%. Uncertainties in the acceptance and efficiency of the counters caused a systematic error of $\sim 20\%$ to the absolute value of η and Υ . The intensity at the laser focus deduced by this method is in good agreement with the average value calculated from the measured laser parameters.

Fig. 5 shows the yield of positrons/laser shot (R_{e^+}) as a function of Υ . The solid line is a power law fit to the data and gives

$$R_{e^+} \propto \Upsilon^{10.0 \pm 0.4 \text{ (stat.)} \pm 0.4 \text{ (syst.)}}, \quad (8)$$

where the statistical error is from the fit and the systematic error was estimated

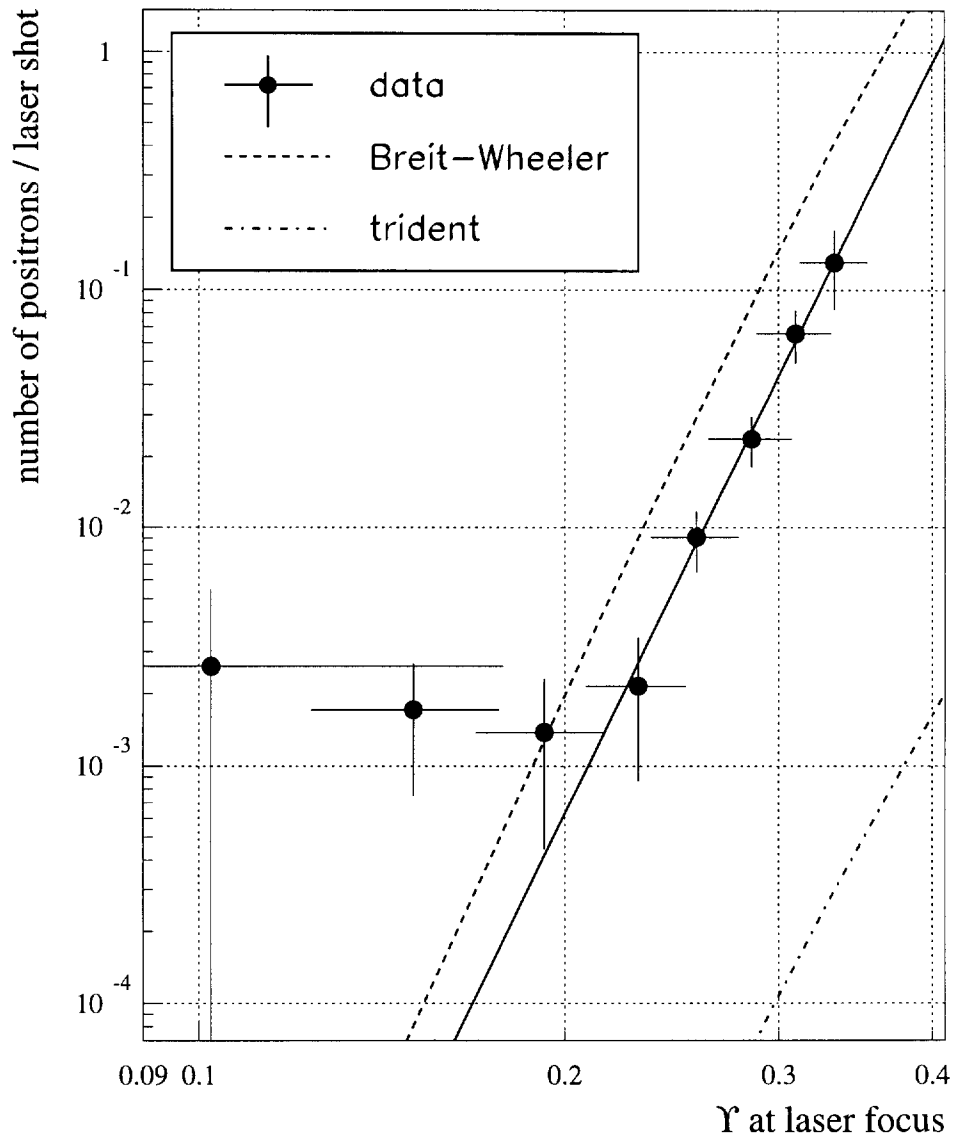


FIGURE 5: Dependence of the positron rate on the laser intensity. The solid line shows a power law fit to the data. The dashed line is the prediction based on the numerical integration of the two-step Breit-Wheeler process, (6) followed by (3). The shift between the data and this simulation is well within the combined effect of the systematic uncertainty of 45% in the e -laser overlap efficiency and the 20% uncertainty in the absolute value of Υ . The dash-dot line represents the calculation for the one-step trident process (10) with an intermediate virtual photon.

by choosing different bin sizes in Υ . Thus, the observed positron production rate is highly nonlinear, varying as the 10^{th} power of the electric field strength. This is in good agreement with expectations as on average $n = 5.5$ photons are needed to produce a pair (1 in reaction (6) and 4.5 in (3)) and the rate of multiphoton reactions involving n laser photons is approximately proportional to Υ^{2n} . Several points at low values of Υ seen in Fig. (5), while statistically consistent with the fit in Eq. (8), indicate a possible residual background of $\sim 2 \times 10^{-3}$ positrons/laser shot in the data sample.

The dashed curve in Fig. 5 shows the prediction based on the numerical integration of the two-step Breit-Wheeler process, (6) followed by (3), and confirms the observed rate dependence on Υ . The simulated rate has been reduced by a factor of 0.35 to account for the average efficiency in e -laser overlap of $35\% \pm 15\%$ as deduced from the Compton monitors EC37, N2 and N3. The apparent shift between the data and this simulation is well within the combined effect of the systematic uncertainty in the e -laser overlap efficiency and the 20% uncertainty in the absolute value of Υ .

To confirm the form of Eq. (5) we plot the yield of positrons/laser shot (R_{e^+}) as a function of $1/\Upsilon$ in Fig. 6. The solid line is an exponential fit to the data and gives

$$R_{e^+} \propto \exp[(-2.8 \pm 0.2 \text{ (stat.)} \pm 0.2 \text{ (syst.)})/\Upsilon], \quad (9)$$

with a χ^2 per degree of freedom of 1.13. This result is in close agreement with the prediction of Eq. (5).

Although we have demonstrated a signal of positron production associated with scattering of laser light we cannot immediately distinguish positrons from reaction (3) from those originating in the trident process

$$e + n\omega_0 \rightarrow e'e^+e^-, \quad (10)$$

which is the Bethe-Heitler process for an electron target. A complete theory of reaction (10) does not exist at present so we have performed calculations based on a two-step model in which the beam electron emits a virtual-photon according to the Weizsäcker-Williams approximation and the virtual photon combines with laser photons to yield electron-positron pairs according to the theory of the multiphoton Breit-Wheeler process (3). This is distinct from the real-photon calculation previously discussed. The results of this simulation indicate that for the interaction geometry of the present experiment and the values of Υ achieved, the trident process is suppressed by more than three orders of magnitude. The expected trident rate, also corrected for e -laser overlap efficiency, is shown in Fig. 5 as the dash-dot line.

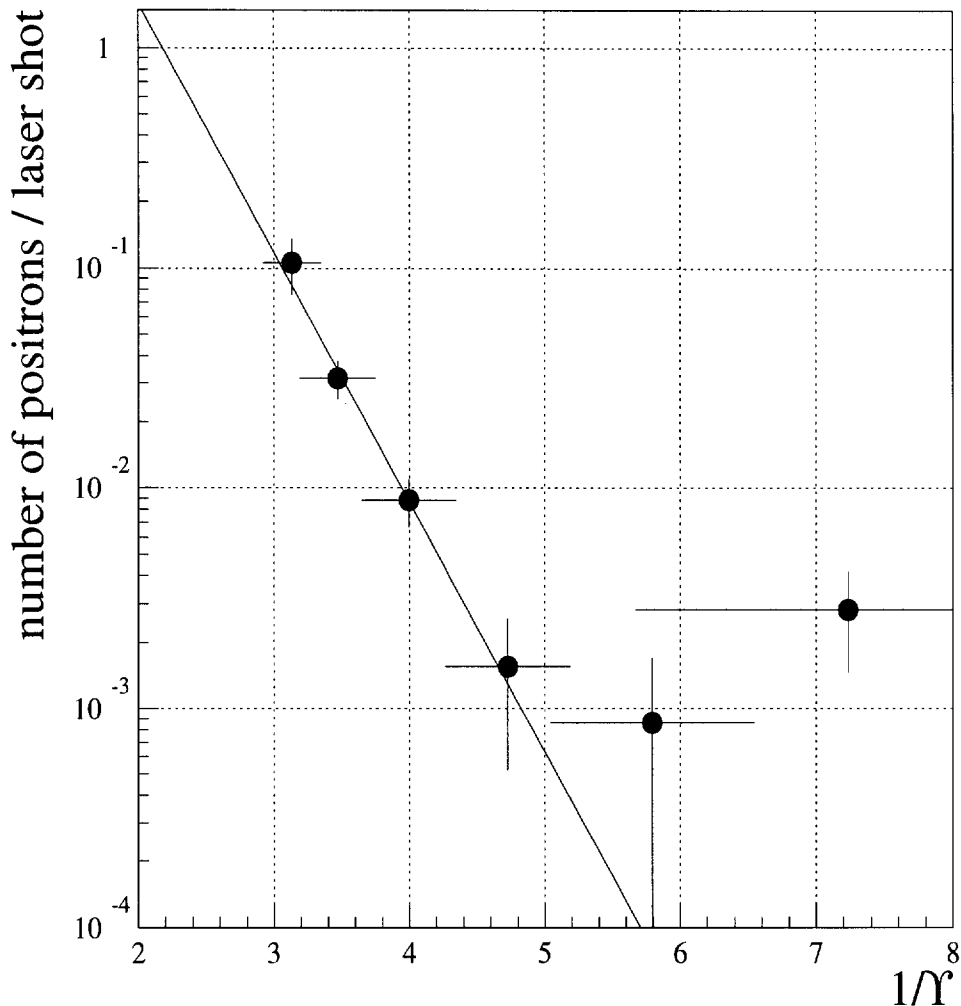


FIGURE 6: Positron yield per laser shot *vs.* $1/\Upsilon$. The solid line shows an exponential fit to the data and confirms the form predicted by Eq. (5).

CONCLUSION

These results, as well as those presented in Ref. [17], confirm the validity of the formalism of strong-field QED and show that the observed rates for the multiphoton reactions (3) and (6) are in agreement with the predicted values. Furthermore these results are the first demonstration of breakdown of the vacuum by an intense electromagnetic wave, and they are the first observation of photon-photon scattering with real photons.

ACKNOWLEDGMENTS

We thank the SLAC staff for its extensive support of this experiment. The laser system could not have been completed without support from members of the Laboratory for Laser Energetics at U. Rochester. T. Blalock was instrumental in the construction of the laser system and its installation at SLAC. We also thank U. Haug, A. Kuzmich and D. Strozzi for participation in recent data collection, and A. Odian and P. Chen for many useful conversations. KTM wishes to thank J.A. Wheeler for continued inspiration.

REFERENCES

1. C.D. Anderson, *Science* **76**, 238 (1932); *Phys. Rev.* **43**, 491 (1933).
2. H.A. Bethe and W. Heitler, *Proc. Roy. Soc.* **A146**, 83 (1934).
3. G. Breit and J.A. Wheeler, *Phys. Rev.* **46**, 1087 (1934).
4. O.C. De Jager *et al.*, *Nature* **369**, 294 (1994).
5. H.R. Reiss, *J. Math. Phys.* **3**, 59 (1962).
6. A.I. Nikishov and V.I. Ritus, *Sov. Phys. JETP* **19**, 529, 1191 (1964); **20**, 757 (1965).
7. N.B. Narozhny *et al.*, *Sov. Phys. JETP* **20**, 622 (1965).
8. R.H. Milburn, *Phys. Rev. Lett.* **10**, 75 (1963).
9. D. Strickland and G. Mourou, *Opt. Comm.* **55**, 447 (1985).
10. F. Sauter, *Z. Phys.* **69**, 742 (1931).
11. W. Heisenberg and H. Euler, *Z. Phys.* **98**, 718 (1936).
12. W. Greiner and J. Reinhardt, *Quantum Electrodynamics*, Berlin, Springer, 1992, p. 285.
13. *Nucl. Instr. and Meth.* **355**, (1995).
14. K.O. Mikaelian, *Phys. Rev. D* **17**, 750 (1978); **30**, 1115 (1984).
15. I.F. Ginzburg *et al.*, *Nucl. Phys.* **B228**, 285 (1983).
16. P. Chen and R.B. Palmer, SLAC-PUB-5966 (Nov. 1992).
17. C. Bula *et al.*, *Phys. Rev. Lett.* **76**, 3116 (1996).
18. T. Kotseroglou, Ph.D. thesis, U. Rochester, UR-1459 (Jan. 1996).
19. V. Balakin *et al.*, *Phys. Rev. Lett.* **74**, 2479 (1995).
20. C. Bamber *et al.*, U. Rochester preprint UR-1428 (June 1995).
21. S.J. Boege, Ph.D. thesis, U. Rochester, UR-1458 (Jan. 1996).
22. T. Kotseroglou *et al.*, *Nucl. Instr. and Meth. A* **383**, 309 (1996).

